Chiral Self-Dimerization of Vanadium Complexes on a SiO_2 Surface for Asymmetric Catalytic Coupling of 2-Naphthol: Structure, Performance, and Mechanism

Mizuki Tada,[†] Norimichi Kojima,[‡] Yasuo Izumi,[§] Toshiaki Taniike,[†] and Yasuhiro Iwasawa*[,†]

Department of Chemistry, Graduate School of Science, The University of Tokyo, Hongo, Bunkyo-ku, Tokyo, 113-0033, Japan, Department of Basic Science, Graduate School of Arts and Sciences, The University of Tokyo, Komaba, Meguro-ku, Tokyo, 153-8902, Japan, and Interdisciplinary Graduate School of Science and Engineering, Tokyo Institute of Technology, Nagatsuta, Midori-ku, Yokohama, 226-8502, Japan

Received: December 16, 2004; In Final Form: March 26, 2005

Vanadium monomers with chiral tridentate Schiff-base ligands were supported on SiO_2 through a chemical reaction with surface silanols, where we found a new chirality creation by the self-dimerization of the vanadyl complexes on the surface. The chiral self-dimerization and the role of surface silanols in the self-assembly were investigated by means of X-ray absorption near-edge structure (XANES), extended X-ray absorption fine structure (EXAFS), diffuse-reflectance ultraviolet/visible (DR−UV/VIS), X-ray photoelectron spectroscopy (XPS), Fourier transform infrared (FT-IR), electron spin resonance (ESR), and density functional theory (DFT) calculations. The surface vanadyl complexes had a distorted square-pyramidal conformation with a V═O bond. FT-IR spectra revealed that the Ph−O moiety of Schiff-base ligands was converted to Ph−OH by a surface-concerted reaction between the vanadium precursors and surface SiOH groups. The Ph−OH in an attached vanadyl complex interacted with a COO moiety of another vanadyl complex by hydrogen bonding to form a self-dimerized structure at the surface. The interatomic distance of V−V in the surface self-assembly was evaluated to be 0.40 ± 0.05 nm by ESR after O_2 adsorption. The self-dimerized V structure on SiO_2 was modeled by DFT calculations, which demonstrated that two vanadium monomers with Ph−OH linked together by two hydrogen bonds and their V═O groups were directed opposite to each other. The surface self-dimerization of the vanadium precursors fixes the direction of the V═O bond and the plane of the Schiff-base ligand. Thus, a new chiral reaction field was created by two types of chirality: the chiral Schiff-base ligand and the chiral V center. We have also found that the chiral self-dimerized vanadyl complexes exhibit remarkable catalytic performance for the asymmetric oxidative coupling of 2-naphthol: 96% conversion, 100% selectivity to 1,1′-binaphthol (BINOL), and 90% enantiomeric excess (ee). Increasing the vanadium loading on SiO_2 caused a dramatic swell of enantioselectivity, and the maximum 90% ee was observed on the supported catalyst with the full coverage of the vanadyl complex (3.4 wt % vanadium). This value is equivalent to the maximum ee reported in homogeneous catalysis for the coupling reaction. Furthermore, the supported vanadium dimers were reusable without loss of the catalytic performance. To our knowledge, this is the first heterogeneous catalyst for the asymmetric oxidative coupling of 2-naphthol.

1. Introduction

Hundreds of optically active substances are composites, and asymmetric catalysis has an important role in chemical syntheses. The development of asymmetric catalysis has been cultivated in homogeneous metal complexes for the last two decades.[1,2] Vast numbers of chiral ligands were designed and prepared for asymmetric catalysis by homogeneous metal complexes, and the exact choice of ligands and the precise geometric regulation on metal sites make high enantioselectivity possible. Now, the exploitation of new optically pure ligands is the most productive way to increase enantioselectivity. The contribution of heterogeneous catalysts to asymmetric catalysis has been quite inferior to that of homogeneous catalysts, although their multifunctional reaction properties with potential applications are worthy of special mention. The simple adaptation of homogeneous asymmetric systems to heterogeneous system is generally not successful. Novel design and control of heterogeneous surfaces are keys to succeed in heterogeneous asymmetric catalysis.

1,1′-Binaphthol (BINOL) and its derivatives have been utilized as versatile chiral sources for asymmetric catalysis, and efficient catalysts for their syntheses are ultimately requested in many chemical fields.[3−6] The oxidative coupling of 2-naphthols is a direct synthesis of BINOL derivatives,[7,8] and some transition metals such as copper,[9,10] iron,[10,11] and manganese[12] are known as active metals for the reaction. However, only few studies on homogeneous metal complexes have been reported for the asymmetric coupling of 2-naphthols.[13−20] To our knowledge, there is no report on heterogeneous asymmetric catalysts for the catalytic coupling reaction.

* Corresponding author: Tel: +81-3-5841-4363. Fax: +81-3-5800-6892. E-mail: iwasawa@chem.s.u-tokyo.ac.jp.

[†] Department of Chemistry, Graduate School of Science, The University of Tokyo.

[‡] Department of Basic Science, Graduate School of Arts and Sciences, The University of Tokyo.

[§] Tokyo Institute of Technology.

10.1021/jp044277n CCC: $30.25
Published on Web 04/26/2005

In the last three decades, we have designed and successfully prepared a variety of supported metal complexes on oxide surfaces, which exhibit unique catalytic activities and selectivities that are different from those of their homogeneous analogues.[21−27] With the aid of several sophisticated spectroscopic techniques, the structures and roles of catalytically active species on surfaces have been characterized and identified.[21−37] Chemical interactions between metal complexes and oxide surfaces can provide new reactivity of metal species by the construction of spatially controlled reaction environment and the formation of unsaturated active metal species, leading to high catalytic activity, selectivity, and durability.[33−37]

Chiral vanadyl complexes with a V═O moiety have stimulated great interest in both catalysts for oxidative coupling[6−20] and some enzymes.[38−42] We found that a chiral structure is created by the surface-mediated self-dimerization of vanadyl complexes on SiO_2, and the designed vanadyl complexes supported on the surface are active and enantioselective for the asymmetric oxidative coupling of 2-naphthol: 96% conversion, 100% selectivity to BINOL, and 90% enantiomeric excess (ee) to (R)-BINOL.[43] The precursor complexes exhibited only 0%−15% conversion and 0%−8% ee. This is the first heterogeneous catalyst for the asymmetric oxidative coupling of 2-naphthol. In this paper, we report the detail of the new chirality creation by the chiral self-dimerization of vanadyl complexes on a SiO_2 surface, its characterization by X-ray absorption near-edge spectroscopy (XANES), extendsed X-ray absorption fine structure (EXAFS), diffuse-reflectance ultraviolet/visible (DR−UV/VIS), X-ray photoelectron spectroscopy (XPS), Fourier transform infrared (FT-IR), electron spin resonance (ESR), and density functional theory (DFT) calculations, and their catalytic performances for the asymmetric coupling. Surface silanol groups are demonstrated to have crucial roles in not only attaching the vanadyl complexes but also their structural reconstruction on the surface: the chiral self-dimerization. Thus, the surface creates new chirality on the vanadyl complexes, which is not possible in homogeneous systems, because of the quite low energy difference between chiral isomers in solutions.[44−46] We have also investigated the mechanistic aspects of the coupling reaction on the surface.

2. Experimental Section

Synthesis of Six Vanadium Monomer Precursors with Schiff Bases. All chemicals were purchased from Wako Chemicals. Vanadium monomer precursors coordinated with chiral α-amino acid-based Schiff bases were synthesized by a similar method reported previously.[47] Here, we briefly summarize the procedure of the preparation: α-amino acid (L-valine, L-isoleucine, L-leucine, L-*tert*-leucine, and L-phenylalanine) and sodium acetate were dissolved in distilled water. Salicylaldehyde or hydroxy naphthaldehyde in ethanol was added to the solution, and an aqueous solution of vanadyl sulfate was slowly added dropwise with vigorous stirring. The obtained gray precipitate was collected and washed with distilled water and a mixture of ethanol and ethyl ether. The compound was dried at a temperature of 313 K under vacuum. Recrystallization was performed in methanol/water, followed by evacuation at 313 K.

Preparation of Supported Vanadyl Complexes. The vanadium monomer complexes were dissolved in dehydrated ethanol and impregnated under N_2 atmosphere with SiO_2 (Aerosil 200), Al_2O_3 (Allon C), and TiO_2 (P-25) precalcined at 773 K for 2 h. After stirring for 1 h at ambient temperature, the solvent was evaporated, and the sample was dried under vacuum for 7 h. Vanadium loadings were changed in the range of 0.3−3.4 wt %, which were determined by X-ray fluorescence (XRF).

Transmission and Diffuse-Reflectance Ultraviolet/Visible (UV/VIS) Region. UV/VIS spectra were measured on a JASCO model V-550-DS spectrometer at room temperature. A vanadium precursor was dissolved in ethanol and measured in transmission mode. The supported vanadyl complexes were enclosed in a quartz cell under N_2 atmosphere and evacuated under vacuum. The supported vanadyl complexes were treated with 2-naphthol in toluene under a N_2 atmosphere, and the solvent was evacuated.

Fourier Transform Infrared (FT-IR) Spectroscopy. FT-IR spectra were recorded on a JEOL model JIR-7000 spectrometer. Isotope-labeled and nonlabeled L-leucine-derived vanadium precursors were prepared in a similar way: the original complex without any isotope labeling, the complex labeled with ^{13}C at the position of C═O, and the complex with both ^{13}C at C═O and ^{15}N at C═N.

X-ray Photoelectron Spectroscopy (XPS). XPS spectra were recorded on a Rigaku model XPS-7000 apparatus at a base pressure of 1×10^{-7} Pa. The X-ray source, voltage, and current were Mg Kα, 10 kV, and 30 mA, respectively. Binding energies were referred to C 1s (284.8 eV) and Si 2p (103.4 eV). The peak areas of V $2p_{5/2}$ were normalized with references to those of O 1s and Si 2p.

Electron Spin Resonance (ESR). ESR X-band spectra for the supported vanadium catalysts (0.3−3.4 wt %) were recorded on JEOL model JES−RE2X equipment at 6 K. The first ESR spectrum was measured under vacuum, and the second spectrum was measured in the presence of O_2. The adsorption of oxygen was performed twice after evacuation at 293 K. These spectra were calibrated with MnO_2. The changes in ESR spectra were investigated for both forbidden half-field ($|\Delta Ms| = 2$) and allowed ($|\Delta Ms| = 1$) transitions. The interatomic distance of V−V was evaluated by the relative intensities of a half-field transition ($|\Delta Ms| = 2$) to a main ($|\Delta Ms| = 1$) transition, which are inversely proportional to the sixth power of the V−V distance (r).[48] Two vanadium dimers with O═V···V═O conformations (two V═O are directed opposite), $K_4[VO(cit)]_2 \cdot 6H_2O$ (where cit denotes citrate) with a V−V distance of $r = 0.3301$ nm,[49] and $Na_4[VO(d\text{-tart})]_2$ (where tart denotes tartrate) with a V−V distance of $r = 0.435$ nm[50,51] were synthesized for references and the constant of the inverse proportion was estimated by the two references with different V−V distances. The V−V distances of the supported vanadium catalysts before and after the coordination of 2-naphthol were estimated by O_2 adsorption.

X-ray Absorption Fine Structure (XAFS) Measurements. XAFS spectra at the V K-edge were measured in transmission mode at 15 K at the BL-9A station of the Photon Factory in the Institute of Materials Structure Science, High Energy Accelerator Research Organization (KEK−IMSS−PF). The energy and current of electrons in the storage ring were 2.5 GeV and 300−450 mA, respectively. X-rays from the storage ring were monochromatized by Si(111) double crystals, and higher harmonics were rejected by rhodium-coated cylindrically bent mirrors. Ionization chambers filled with N_2/He (30/70) and pure N_2 gases were used to monitor incident and transmitted X-rays, respectively. The XANES spectra were calibrated with the pre-edge peak positions of spectra for V_2O_5 and $VOSO_4$ as 5470.6 and 5469.8 eV, respectively.[52] The EXAFS spectra were analyzed with the UWXAFS package.[53] The threshold energy (E_0) was tentatively set at the inflection point of the absorption edge. The background was subtracted by the AUTOBK program, and the obtained k^3-weighted EXAFS data were Fourier-transformed into R-space. Curve-

SCHEME 1: Preparation Route of the Chiral Self-Dimerized Vanadium Complexes on SiO_2[a]

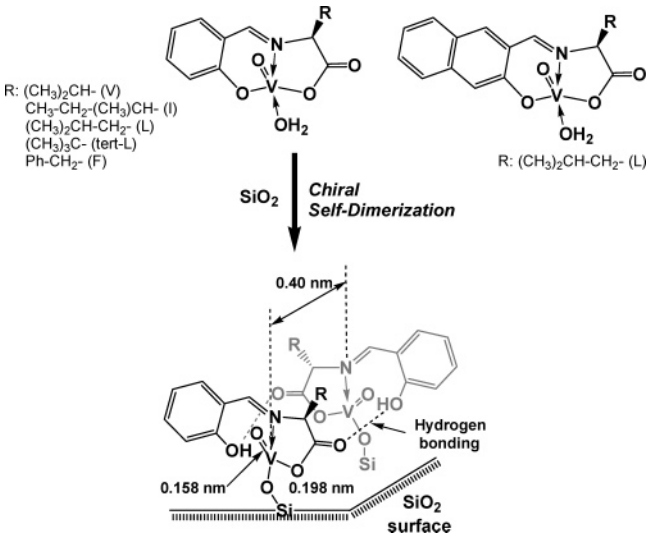

[a] Two vanadium monomers are dimerized through two sets of hydrogen bonds between Ph−OH and COO with each other. The V−V distance of 0.40 nm was evaluated in the presence of O_2.

fitting analysis was performed using the FEFFIT program in the *R*-space with two shells: short V═O and long V−O bonds. The coordination of the V═O bond was fixed as 1.0, based on the results of XANES. Phase shifts and backscattering amplitudes were calculated by the FEFF8 code.[54] The coefficient of multiphoton effect (S_0^2) was estimated by curve-fitting for $VOSO_4$ with a V═O bond.

Density Functional Theory (DFT) Calculation. All ab initio calculations were performed using a commercially available density functional code (Dmol3 4.2.1[55]) on a Cerius 2.4.2 graphical interface (Accelrys, USA), where exchange-correlation interaction was treated by the Perdew-Wang 91 functional (PW91) within a generalized gradient approximation.[56] We used valence electrons double-numeric basis sets with polarization functions (DNP), the size of which is comparable to 6-31G**, and core electrons effective core potentials (ECP). Wave functions that contain the contribution of V atoms include the effects of spin polarization. Harmonic frequencies were calculated based on the numerical differentiations of total energy.

The Oxidative Coupling of 2-Naphthol. The oxidative coupling of 2-naphthol was performed on both homogeneous and heterogeneous vanadium catalysts in the temperature range of 263−293 K under O_2 atmosphere (101.3 kPa). The molar ratio of vanadium dimer and 2-naphthol was basically fixed to $^1/_{36}$ and 5 mL of solvent (toluene or chloroform) was used. The dependency of the catalytic activity on 2-naphthol concentration was investigated in a toluene solution with the fixed amount of a supported vanadium catalyst. The reaction in the absence of oxygen was also performed under a N_2 atmosphere.

3. Results

Supported vanadyl complexes were prepared on three oxides (SiO_2, Al_2O_3, and TiO_2), using six vanadium monomers with Schiff-base ligands, as presented in Scheme 1. Vanadium loadings were varied from a low concentration (0.3 wt %) up to almost a full monolayer (3.4 wt %). Only SiO_2-supported catalysts were active and completely selective for the asymmetric oxidative coupling of 2-naphthol, as described hereinafter. Thus, the SiO_2-supported vanadyl complexes were characterized well.

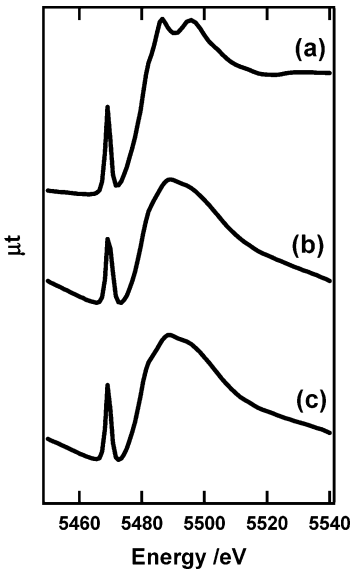

Figure 1. V K-edge XANES spectra for (a) a vanadium precursor (L-leucine), (b) its SiO_2-supported vanadyl complex (3.4 wt % vanadium), and (c) that treated with 2-naphthol.

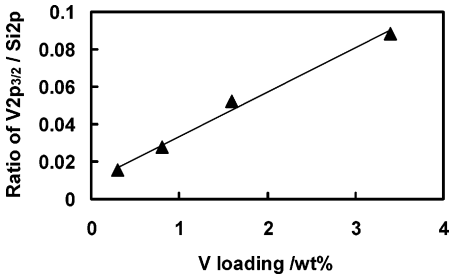

Figure 2. Relationship between the V $2p_{3/2}$ (515.9 eV) XPS peak area and vanadium loading for the SiO_2-supported vanadyl complexes prepared from L-leucine. The peak areas were normalized to Si 2p peak areas.

X-ray Absorption Near-Edge Structure (XANES), Ultraviolet/Visible (UV/VIS), and X-ray Photoelectron Spectroscopy (XPS) Spectra for SiO_2-Supported Vanadium Complexes. Figure 1 shows V K-edge XANES spectra for a vanadium monomer precursor (L-leucine-based Schiff base) (Figure 1a) and its SiO_2-supported vanadyl complex (Figure 1b). Absorption-edge transition is assigned as an electronic transition from V 1s to a V 4p empty state. In the case of V═O complexes, a parity-forbidden transition from V 1s to V 3d is observed as a sharp pre-edge peak, because of the overlapping of V 3d with O 2p[57] and the mixing of V 3d−4p.[52] The pre-edge peak position reflects vanadium valences.[52] A sharp pre-edge peak at 5469.2 eV attributed to the V═O bond for the vanadium precursor (see Figure 1a) did not disappear in the spectrum of the supported vanadyl complex (see Figure 1b), indicating that the V═O double bond remained unchanged when the vanadium precursor was supported on SiO_2. The pre-edge peak position (5469.2 eV) of the supported catalyst was same as that of the precursor. Hence, the valence of the vanadium center is four (V^{4+}) on the surface. No spectral changes were observed upon the coordination of 2-naphthol (see Figure 1c).

A peak of V $2p_{3/2}$ was observed at 515.9 eV in XPS spectra. The peak area of V $2p_{3/2}$, normalized to O 1s and Si 2p peak areas, was plotted against the amount of vanadium loading in Figure 2. The relative peak area linearly increased in the vanadium loading range of 0.3−3.4 wt %. The binding energies of the V $2p_{3/2}$ were essentially unchanged (515.8−516.0 eV) for the 0.3−3.4 wt % vanadium catalysts. The binding energies

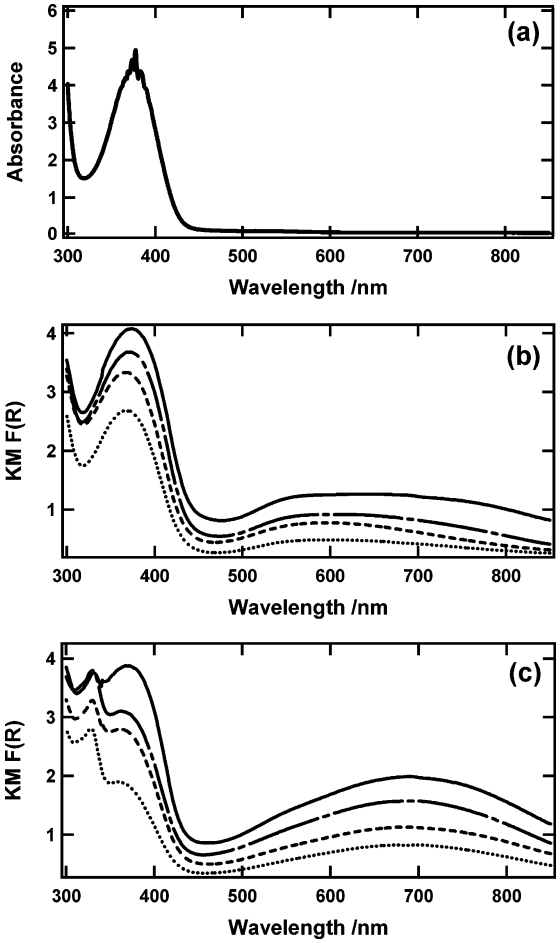

Figure 3. (a) Transmitted UV/VIS spectrum of a vanadium precursor (L-leucine) in ethanol, (b) DR−UV/VIS spectra of the SiO_2-supported vanadium catalysts ((···) 0.3 wt %, (- - -) 0.8 wt %, (-·-·-) 1.6 wt %, and (—) 3.4 wt %), and (c) DR−UV/VIS spectra of those treated with excess 2-naphthol ((···) 0.3 wt %, (- - -) 0.8 wt %, (-·-·-) 1.6 wt %, and (—) 3.4 wt %).

are attributed to those of V^{4+} species; those of V^{3+} of $V(OH)_3$ and V_2O_3 are 514.1 eV[58] and 515.7 eV,[59] respectively, whereas that of $VOSO_4$ (V^{4+}) is 515.9 eV[60] and that of V_2O_5 (V^{5+}) is 516.9 eV.[59] The coordination of 2-naphthol did not change the binding energy (515.9 eV), indicating that the vanadium valence was 4+, in agreement with the XANES results.

Figure 3 shows UV/VIS spectra for the vanadium precursor and the supported vanadyl complexes. A strong absorption at 380 nm was attributed to azomethyne.[61,62] There are no significant peaks at ~600 nm in the UV/VIS spectrum of the vanadium−leucine precursor (see Figure 3a). On SiO_2, a new band at ~550 nm appeared, because of the d−d transition of the vanadium species (see Figure 3b). With increased vanadium loading on SiO_2 (0.3, 0.8, 1.6, and 3.4 wt %), the new peak grew at a similar position, as shown in Figure 3b. After the coordination of 2-naphthol, the peak shifted to 680 nm, and the peak grew as a function of vanadium loading (see Figure 3c).

Structural Parameters by Extended X-ray Absorption Fine Structure (EXAFS). The curve-fitting analysis of V K-edge EXAFS spectra was performed to examine local structures around a vanadium center. Figure 4 shows EXAFS oscillations (denoted with a suffix 1) and their Fourier-transformed EXAFS spectra (denoted with a suffix 2). The curve-fitting results are presented in Table 1. The XANES spectra for both the precursor and the supported vanadyl complex demonstrated the existence of a V═O double bond: thus, the coordination number (CN) of the V═O bond was fixed to be 1.0 for the fitting, to minimize fitting errors. The structure of the vanadium precursor (a L-leucine-based Schiff base) is known by X-ray diffractometry (XRD),[63] and the EXAFS curve-fitting analysis for the vanadium precursor agreed with the XRD data (see parts (a) and (d) in Table 1).

EXAFS data for the supported vanadyl complexes were analyzed in a similar way. A V═O bond length of 0.157 ± 0.001 nm is similar to that of the precursor, whereas the CN of V−O bonds with a length of 0.199 ± 0.002 nm decreased from 3.8 ± 0.4 to 2.8 ± 0.5, as shown in part (b) in Table 1. The decrease in the CN of V−O upon supporting was also observed for 0.8-, 1.6-, and 3.4-wt % vanadium samples, independent of the vanadium loading. Longer-distance bonding was not observed with all the catalysts, indicating that there was no direct V−V bonding in the supported vanadium catalysts.

The treatment of the supported vanadium catalyst with 2-naphthol caused recovery of the CN of V−O bonds to 4.0 ± 0.6 (see part (c) in Table 1). The CN of V−O did not increase after the addition of excess 2-naphthol (the 2-naphthol/vanadium molar ratio is 200). No more 2-naphthol molecules coordinated to the supported vanadyl complex. The V═O double bond length was 0.157 ± 0.002 nm, similar to that of the fresh sample before the 2-naphthol coordination. There was no direct V−V bonding after the coordination of the reactant.

Fourier Trnasform Infrared (FT-IR) Spectra for the Schiff-Base Ligand. All coordination sites of the Schiff-base ligand to the V^{4+} center possess infrared-active functional groups, Ph−O, Ph ring, C═N, and COO, as shown in Scheme 1. Optionally, vanadium monomers coordinated with L-leucine-based Schiff bases were labeled with isotope atoms ^{13}C and ^{15}N. A complex was substituted with ^{13}C═O, and the other complex was substituted with both ^{15}N═C and ^{13}C═O. Table 2 is the summary of the vibration frequencies of these groups, as measured using FT-IR. Three frequencies (1598, 1373, and 1362 cm^{-1}) were assigned as one $\nu_{asym(COO)}$ vibration and two $\nu_{sym(COO)}$ vibrations. The small differences between $\nu_{asym(COO)}$ and $\nu_{sym(COO)}$ (~ 230 cm^{-1}) imply the delocalization of electron density on the C═O bond to O−CO. Indeed, XRD data for its crystal reveals that O═CO links with a H_2O ligand of another vanadyl complex by hydrogen bonding. The 1629 cm^{-1} peak is assigned to $\nu_{(C=N)}$, which is coupled with $\nu_{(Ph)}$, as suggested by DFT calculation of the crystal structure. Four peaks of 1547, 1470, 1447, and 1436 cm^{-1} are referred to $\nu_{(Ph)}$, and, indeed, they were common in the three isotope-labeled complexes (see Table 2). The strong peak at 1290 cm^{-1} is attributed to $\nu_{(Ph-O)}$. The frequencies for the crystal structure were calculated by DFT, which were in agreement with these experimental data.

The IR peaks for the supported catalyst (3.4 wt %) were attributed to $\nu_{(C=N)}$ (1629 cm^{-1}), $\nu_{asym(COO)}$ (1602 cm^{-1}), $\nu_{(Ph)}$ (1554, 1548, 1471, and 1452 cm^{-1}), $\nu_{sym(COO)}$ (1370 cm^{-1}), and $\nu_{(Ph-O)}$ (1391 cm^{-1}), as shown in Table 2. The difference between $\nu_{asym(COO)}$ and $\nu_{sym(COO)}$ was also small, which implies that there is hydrogen bonding on C═O to delocalize electron density. The $\nu_{(C=N)}$, $\nu_{asym(COO)}$, and $\nu_{sym(COO)}$ vibrations were very similar to those of the precursor, indicating no significant change in the original coordination of these groups upon supporting. On the other hand, the noted four $\nu_{(Ph)}$ peaks were different than those of the precursor, in both their positions and relative intensities. The peak at 1547 cm^{-1} for the precursor split into two peaks, at 1554 and 1548 cm^{-1}. The relative intensities of the other three peaks at 1470, 1447, and 1436 cm^{-1} were 1, 2, and 1.4 for the precursor, whereas the

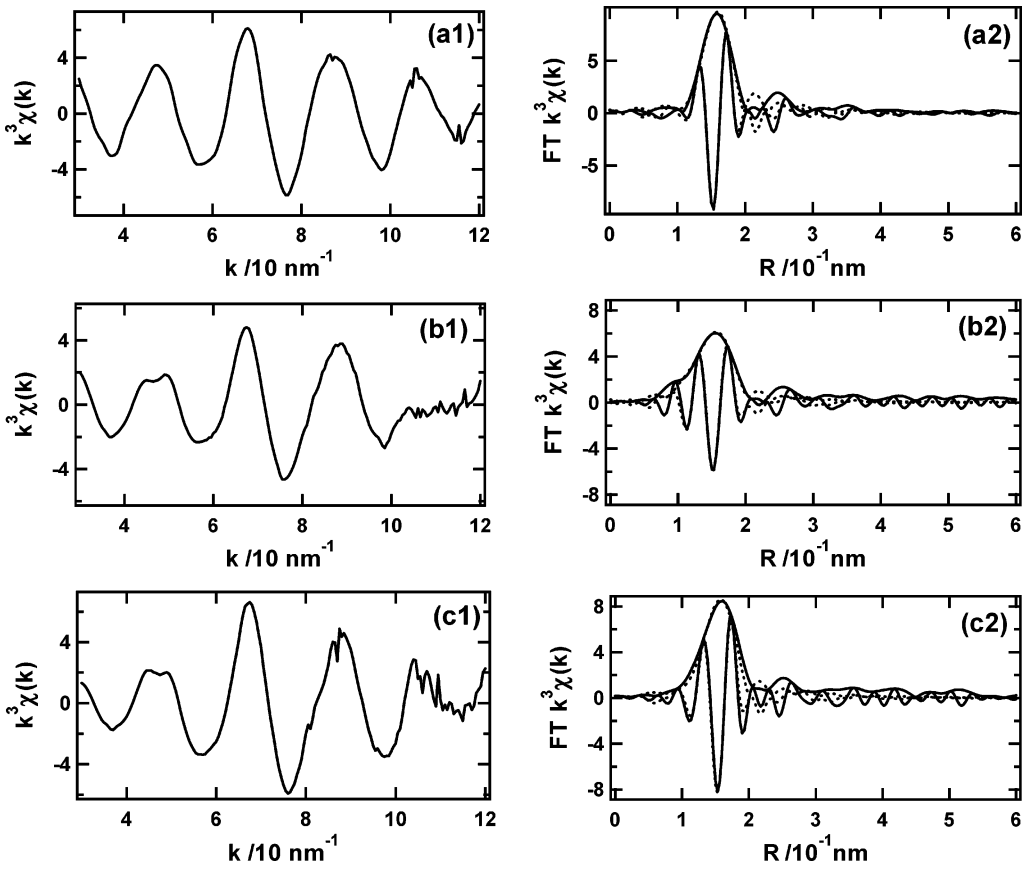

Figure 4. V K-edge EXAFS oscillations (denoted by the suffix 1) and their associated Fourier-transformed spectra (denoted by the suffix 2) for (a) a vanadium precursor (L-leucine), (b) the supported vanadyl complex on SiO_2 (3.4 wt % vanadium), and (c) that treated with 2-naphthol, measured at 16 K. Solid lines and dotted lines in the FT spectra represent observed and fitted spectra for absolute and imaginary parts, respectively.

TABLE 1: Curve-Fitting Results of Fourier Transformed EXAFS Spectra at the V K-edge for a Vanadium Precursor (L-Leucine), Its Fresh Supported Vanadium Complex (3.4 wt % Vanadium), and That Treated with 2-Naphthol, Measured at 16 K, and Crystallographic Structural Parameters by XRD

shell[a]	coordination number	distance (nm)	σ^2 (nm^2)
	(a) Precursor, $k = 30-120$ nm^{-1}, $R = 0.10-0.20$ nm, $R_f = 0.34\%$		
V═O	1.0	0.158 ± 0.001	$(3 \pm 2) \times 10^{-5}$
V−O	3.8 ± 0.4	0.198 ± 0.001	$(1 \pm 1) \times 10^{-5}$
	(b) Supported Vanadium Complex, $k = 30-120$ nm^{-1}, $R = 0.10-0.20$ nm, $R_f = 0.87\%$		
V═O	1.0	0.157 ± 0.001	$(1 \pm 1) \times 10^{-5}$
V−O	2.8 ± 0.5	0.199 ± 0.002	$(3 \pm 2) \times 10^{-5}$
	(c) Treated with 2-Naphthol, $k = 30-120$ nm^{-1}, $R = 0.10-0.20$ nm, $R_f = 1.70\%$		
V═O	1.0	0.157 ± 0.002	$(1 \pm 2) \times 10^{-5}$
V−O	4.0 ± 0.6	0.199 ± 0.002	$(2 \pm 2) \times 10^{-5}$
	(d) Crystal (XRD)[b]		
V═O	1	0.1589	
V−OPh	1	0.1921	
V−N	1	0.2043	
V−OCO	1	0.1975	
V−OH_2	1	0.2008	

[a] The coordination number of V═O was fixed to be unity. [b] From ref 63.

peak at 1436 cm^{-1} disappeared for the supported complex and the relative intensities of the former two peaks were 1 and 2.7, respectively. Furthermore, the $\nu_{(Ph-O)}$ vibration at 1290 cm^{-1} for the precursor dramatically shifted to 1391 cm^{-1} upon supporting. Such a large shift was observed between Ph−ONa and Ph−OH; the $\nu_{(Ph-O)}$ of the ionized molecule Ph−ONa is located at 1309 cm^{-1}, whereas the $\nu_{(Ph-O)}$ of Ph−OH coupled with a $\nu_{(OH)}$ vibration is located at 1373 cm^{-1}. Therefore, the large shift of $\nu_{(Ph-O)}$ and the changes in the intensity ratio of $\nu_{(Ph)}$ were caused by the structural reconstruction of the Ph−O coordination to produce new Ph−OH that was promoted by proton transfer from SiOH. The entire data set for the behaviors of other vibrations reveal that the supported vanadyl complex possesses V ← N coordination, V−OCO bonding, and Ph−OH. Similar results were obtained for 0.3-, 0.8-, 1.6- and 3.4-wt % SiO_2-supported vanadyl complexes.

Evaluation of the V−V Interatomic Distance by Electron Spin Resonance (ESR). Figure 5 shows X-band ESR spectra at 6 K for the L-leucine-based vanadium precursor (panel A), the supported vanadyl complex (3.4 wt % vanadium) (panels b and B), and that treated with 2-naphthol (panels c and C). Hyperfine signals for the precursor in methanol were observed due to d^1 configuration of the V^{4+} ions (panel a). The relationships $g_{\|} < g_{\perp}$ and $A_{\|} \gg A_{\perp}$ demonstrate an axially

TABLE 2: Vibration Frequencies Measured for Isotope Nonlabeled and Isotope-Labeled L-Leucine-Based Vanadium Complexes[a] and the Supported Vanadium Complex (L-Leucine),[b] Using Fourier Transform Infrared (FT-IR) Spectroscopy

vibration mode	^{12}C, ^{14}N	^{13}C, ^{14}N	^{13}C, ^{15}N	supported vanadium complex[b]
$\nu_{(C=N)}$	1629	1632	1617	1629
$\nu_{asym\ (COO)}$	1598	1560	1559	1602
$\nu_{(Ph)}$	1547	1548	1546	1554
				1548
$\nu_{(Ph)}$[c]	1470	1470	1470	1471
$\nu_{(Ph)}$[c]	1447	1447	1446	1452
$\nu_{(Ph)}$[c]	1436	1435	1435	
$\nu_{sym\ (COO)}$	1373	1353	1351	1370
	1362	1330	1330	negligible
$\nu_{(Ph-O)}$	1290	1289	1290	1391
$\nu_{(V=O)}$	1007	1006	1007	ND[d]

[a] KBr disk. [b] Neat disk, containing 3.4 wt % vanadium. [c] Relative intensity of the three peaks (1470/1448/1436 cm^{-1}) changed from 1/2.0/1.4 to 1/2.7/0 after the supporting. [d] Not determined, because of the large SiO_2 background.

compressed d^1_{xy} configuration of the V=O complex.[64−66] For the vanadyl complexes supported on SiO_2, two different signals were observed in panel b1 of Figure 5. A broad signal was superposed with the hyperfine feature that represented the d^1_{xy} configuration, and the hyperfine coupling constants were $g_{\|} = 1.948$, $A_{\|} = 17.01\ cm^{-1}$, and $g_{\perp} = 1.991$, $A_{\perp} = 6.49\ cm^{-1}$. Its half-field signal was negligible, as shown in panel B of Figure 5.

Oxygen is necessary for the oxidative coupling of 2-naphthol. The amount of adsorbed oxygen at 293 K was negligible for all the supported vanadium catalysts (0.3−3.4 wt %) in the pressure range of 0−50 kPa. At 195 K, the amount of adsorbed oxygen increased to ~0.2 O_2 per vanadium dimer for all of the vanadium-loading catalysts. The similar amounts of adsorbed oxygen in all the catalysts indicate that the similar O_2-adsorbed structure is formed on SiO_2 in the vanadium-loading range of 0.3−3.4 wt %. The O_2 adsorption was totally reversible on the supported vanadyl complexes. After the coordination of 2-naphthol, a similar amount of oxygen was adsorbed on the supported vanadyl complex (3.4 wt %) and the process was also reversible. Thus, we measured the ESR spectra after O_2 adsorption on the supported vanadyl complexes at 6 K, where the complexes may be saturated with adsorbed O_2. The adsorption of O_2 on the supported vanadyl complex dramatically increased the broad signal, as shown in panel b1 of Figure 5. A new peak also appeared at the half field of the main signal, which was attributed to a forbidden transition, the half band of the $|\Delta Ms| = 2$ half band (panel B of Figure 5). The transition ($|\Delta Ms| = 2$) is normally forbidden; however, the triplet state of two d^1 electrons can be observed as a weak transition around half-field position when two metal species are located nearby. Thus, these signals prove the existence of a V−V interaction stimulated by the O_2 adsorption. The ratio of the intensity of the $|\Delta Ms| = 2$ half band to that of the $|\Delta Ms| = 1$ half band is related to the sixth power of the interatomic distance of V−V as follows:[48]

$$\frac{\text{Intensity}\ (|\Delta Ms| = 2)}{\text{Intensity}\ (|\Delta Ms| = 1)} = \text{Cr}^{-6} \qquad (1)$$

where r is the V−V distance and C is a constant. Based on two V d^1 dimers with O=V···V=O coupled structures, whose V=O structures are directed outside of V−V, $K_4[VO(cit)]_2 \cdot 6H_2O$ (with a V−V distance of $r = 0.3301$ nm)[49] and $Na_4[VO(d\text{-tart})]_2$ (with a V−V distance of $r = 0.435$ nm)[50,51] were used as references and the relative constant C was determined. The V−V distance of the supported vanadyl complex (3.4 wt % vanadium) was evaluated to be $r = 0.40 \pm 0.05$ nm, using eq 1. After the evacuation of oxygen at 293 K, the ESR signal returned to the original intensity before the adsorption, as shown in panel b2 in Figure 5 and the half-band signal disappeared. The behavior in the ESR spectra was reversible for the evacuation at 293 K and the readsorption of oxygen at 6 K, as shown in panel b2 in Figure 5.

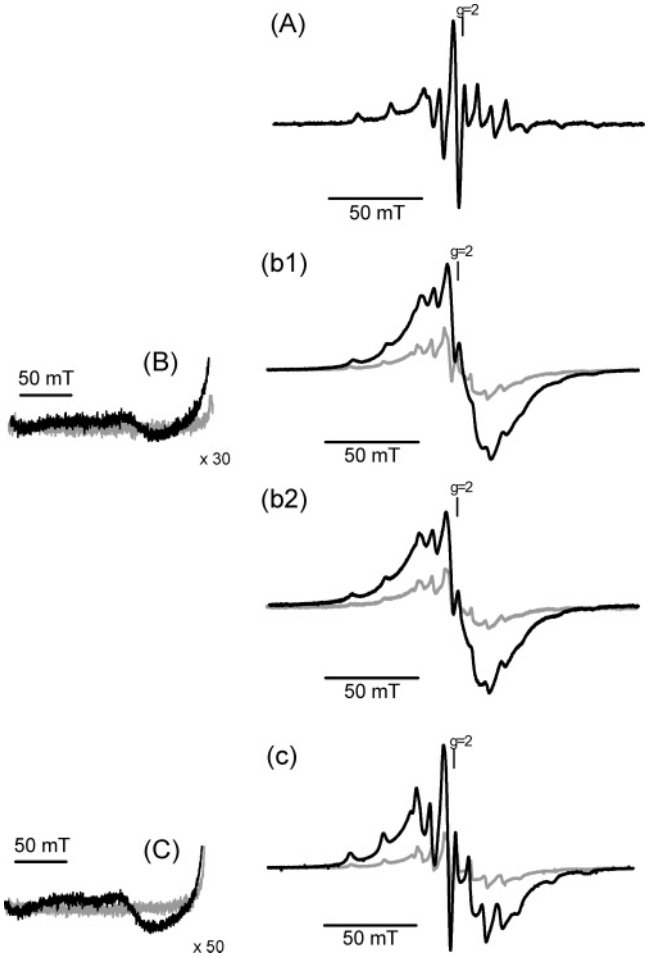

Figure 5. ESR spectra at 6 K for a vanadium precursor (L-leucine) in methanol (panel a), the SiO_2-supported vanadyl complex (3.4 wt % vanadium) in the absence (gray line) and presence (black line) of O_2 (panel b shows the main signal, and panel B shows the half band), and that treated with 2-naphthol in the absence (gray line) and presence (black line) of O_2 (panel c shows the main signal, and panel C shows the half band). ESR measurements after the adsorption and desorption of O_2 were performed twice on the supported vanadyl complex; panel b1 represents data for the first run, and panel b2 represents data for the second run.

The coordination of 2-naphthol maintained the axicially compressed d^1 configuration of the vanadyl complex. A broad signal similar to that before the 2-naphthol coordination was observed (see panel c in Figure 5). The effect of O_2 adsorption on the ESR signal was also observed after the coordination of 2-naphthol: a large increase in the broad main signal and the appearance of a weak half band (see panels C and c in Figure 5). The distance of V−V interaction was evaluated to be $r = 0.40 \pm 0.05$ nm, which is identical to the case of the supported vanadyl complex without 2-naphthol.

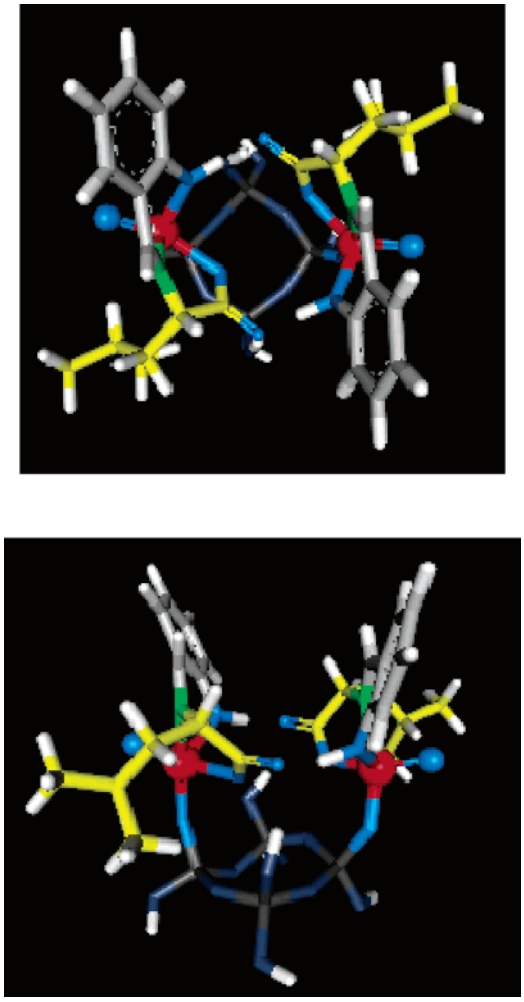

Figure 6. Structure of the self-dimerized vanadyl complex on SiO_2 modeled by DFT; the top panel shows the top view and the bottom panle shows the side view. Legend is as follows: red, vanadium; green, nitrogen; blue, oxygen; gray, Ph ring; and yellow, isobutyl group derived from L-leucine.

Density Functional Theory (DFT) Modeling of the SiO_2-Supported Vanadyl Complex. The structure of the supported vanadyl complex was modeled by DFT calculation, as presented in Figure 6. From the entire set of experimental data, the following conclusions were obtained:

(1) The vanadium valence is four (XANES and XPS),

(2) the vanadium conformation is distorted square pyramidal (XANES and DR−UV/VIS),

(3) the supported vanadyl complex has a coordinatively unsaturated structure with a V═O double bond at 0.157 ± 0.001 nm and three single V−O(N) bonds at 0.199 ± 0.002 nm (XANES and EXAFS),

(4) there is no direct bonding between two V ions (EXAFS and ESR),

(5) the azomethyne backbone of Schiff-base ligands is preserved (DR−UV/VIS),

(6) the coordination of V ← N and the delocalized V ← OCO unchange (FT-IR),

(7) the Ph−OH moiety is formed (FT-IR), and

(8) another vanadyl complex is located at a distance ≥0.4 nm away from a vanadyl complex (ESR).

Therefore, we investigated the following two issues: (i) the chemical attachment of the vanadium precursor on SiO_2, and (ii) the assembly of vanadyl complexes on the surface.

There are four probabilities for a chemical reaction between the vanadium precursor and surface Si−OH; these are depicted in Scheme 2. Judging from the results of FT-IR, the former two models in Scheme 2 (reactions 1 and 2) were excluded; indeed, they were not allowed by DFT either. The decrease in the CN on the V atom and the structural change in the Ph−O moiety suggested that both reactions 3 and 4 in Scheme 2 should be considered: the coordinated H_2O of the vanadium precursor is replaced by Si−OH to release the H_2O that is post-evacuated under vacuum, and a proton of the coordinated Si−OH is transferred to Ph−O to form Ph-OH. In fact, the resultant structure was elucidated to be stable by DFT calculation (V═O, 0.161 nm; V−N, 0.208 nm; V−OCO, 0.195 nm; and V−OSi, 0.192 nm). The Ph−OH was possible to interact with the V atom through hydrogen bonding at 0.212 nm; however, this disagreed with the decrease in the coordination number. Thus, other interactions to dispatch the Ph−OH group from the V atom were examined.

We investigated three possible models of vanadium assembly on SiO_2 suggested by ESR: (a) a model with two V═O bonds directed inside the vanadium dimer (V═O···O═V), (b) a vanadyl-complex assembly arrayed in the same direction (V═O···V═O), and (c) an assembled structure whose V═O are directed opposite to each other (O═V···V═O). These plausible assemblies were built on a silica cluster optimized by DFT, and the entire obtained units were further optimized by DFT. In the cases of structures (a) and (b), positive interaction between two vanadtyl complexes never stabilized any re-conformed structures. In fact, the V═O bond(s) directed inside two V atoms disturbed the assembling of the vanadyl complexes bound to Si−OH. On the other hand, only the third vanadium assembly with O═V···V═O conformation was shown to be stabilized on the surface by DFT. Two vanadyl complexes on a silica cluster dimerized by hydrogen bonding between the formed Ph−OH of a vanadyl complex and the O═CO moiety of the other vanadyl complex are shown in Figure 6. The two sets of hydrogen bonding between two vanadyl complexes stabilized the unsaturated vanadium centers. The differences in the bond distances of O═C and C−O—0.002 nm in the DFT-modeled structure—was similar to that of the vanadium precursor (0.004 nm) and was much different from that of the monomer model (0.011 nm). This delocalization of COO by the hydrogen bonding on the C═O also was in agreement with the COO frequencies presented in Table 2.

A vanadyl complex with α-amino acid-based Schiff ligands have two chiral conformations on the vanadium center; however, their energy difference was calculated to be <1 kJ/mol.[44−46] For this small energy difference, the two chiral isomers coexist with a similar concentration in solution. The surface self-dimerization of the vanadium precursor fixes the direction of V═O and the plane of the Schiff-base ligand, and, as a result, the chirality on a vanadium center is preserved on the surface. The two types of chirality—the chiral Schiff-base ligand and the chirality on a vanadium center—create a new asymmetric reaction space on the supported vanadium-dimer complex, which is unique on the surface.

The cross section of the supported vanadium-dimer complex was estimated from the DFT model of the grafted vanadium monomer. The $(HO)_3Si-O$ moiety was removed from the $Si(OH)_3-O$-grafted model and the cross section of the remaining unit, viewed from the direction of the Si−O(−V) bond normal to the surface, was calculated as the cross section of the vanadium-dimer complex. The vanadium loading of 3.4 wt %

SCHEME 2: Possible Chemical Reactions between a Vanadium Precursor and Surface Si−OH[a]

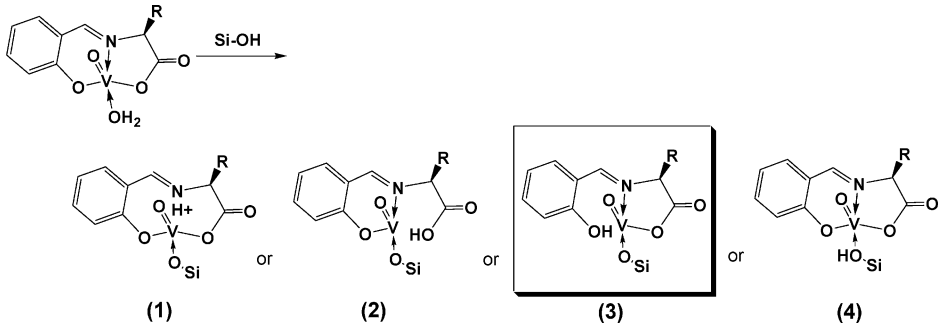

[a] (1) C═NR′ → V + Si−OH → C═NH$^+$R′ + V−OSi. (2) O═CO−V + Si−OH → O═COH + V−OSi. (3) Ph-O−V + Si−OH → Ph−OH + V−OSi. (4) H_2O → V + Si−OH → H_2O + V ← HO−Si.

TABLE 3: Catalytic Activities, Selectivities, and Enantiomeric Excess (ee) in Homogeneous and Heterogeneous Vanadium Catalyses for the Oxidative Coupling of 2-Naphthol[a]

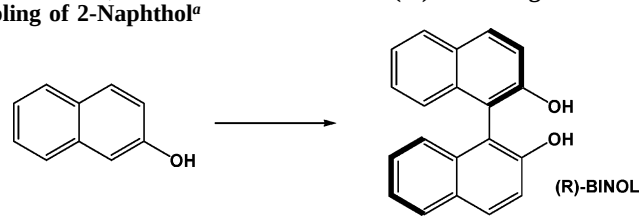

catalyst−ligand[b]	temperature (K)	time (day)	solvent	conversion (%)	selectivity (%)	ee (R) (%)
precursor−L[c]	293	5	$CHCl_3$	0	0	
precursor−L[c,d]	293	3	$CHCl_3$	15	73	8
precursor−L[c,d]	263	9	$CHCl_3$	0	0	
V−L/SiO_2, 0.3 wt %	293	5	$CHCl_3$	76	100	19
V−L/SiO_2, 0.3 wt %	263	5	$CHCl_3$	9	100	54
V−L/SiO_2, 0.3 wt %	293	5	toluene	96	100	13
V−L/SiO_2, 0.3 wt %	263	5	toluene	11	100	32
V−L/Al_2O_3, 1.7 wt %	293	5	$CHCl_3$	69	53	−2
V−L/TiO_2, 0.8 wt %	293	5	$CHCl_3$	52	0	
V−V/SiO_2, 0.3 wt %	293	2	$CHCl_3$	26	100	12
V−V/SiO_2, 0.3 wt %	293	5	toluene	99	100	5
V−V/SiO_2, 0.3 wt %	263	6	toluene	12	100	14
V−I/SiO_2, 0.3 wt %	293	3	$CHCl_3$	37	100	17
V−I/SiO_2, 0.3 wt %	263	5	$CHCl_3$	6	100	51
V−I/SiO_2, 0.3 wt %	293	2	toluene	41	100	21
V−L/SiO_2, 0.3 wt %[e]	293	2	toluene	40	100	13
V−L/SiO_2, 0.3 wt %[e]	263	6	toluene	9	100	31
V−*tert*-L/SiO_2, 0.3 wt %	263	5	toluene	11	100	12
V−F/SiO_2, 0.3 wt %	293	5	$CHCl_3$	81	100	10
V−F/SiO_2, 0.3 wt %	263	5	$CHCl_3$	9	100	56

[a] The vanadium dimer/2-naphthol ratio was $^1/_{36}$, and 100 mg of supported catalysts were used in 5 mL of toluene. [b] L, L-leucine; V, L-valine; I, L-isoleucine; tert-L, L-*tert*-leuicne; and F, L-phenylalanine. [c] Homogeneous reaction. [d] Chlorotrimethylsilane (TMSCl) was added as acid. [e] Hydroxy naphthaldehyde was coordinated instead of salicylaldehyde.

corresponded to full coverage, based on the calculated cross section (0.52 nm^2 per vanadyl complex) on the SiO_2 surface (200 m^2/g).

Catalytic Performances for the Asymmetric Oxidative Coupling of 2-Naphthol. The catalytic oxidative coupling of 2-naphthol was performed on a vanadyl-complex precursor (homogeneous catalyst) and supported vanadyl complexes on SiO_2, Al_2O_3, and TiO_2 (heterogeneous catalysts). Table 3 summarizes the catalytic activities, selectivities, and enantiomeric excess (ee) of homogeneous and heterogeneous vanadium catalysts for the oxidative coupling of 2-naphthol. The homogeneous reactions on a representative L-leucine-based vanadium monomer were performed in $CHCl_3$ in the absence and presence of chlorotrimethylsilane (TMSCl) as an acidic promoter. The vanadium-monomer precursor did not exhibit the catalytic activity without TMSCl. In the presence of TMSCl, the reaction proceeded slightly (15% conversion) at 293 K, but the selectivity to BINOL and ee to (R)-BINOL were quite low (73% and 8%, respectively), as shown in Table 3. Furthermore, a loss of activity was observed. At 263 K, no reaction proceeded after 9 days.

The oxide-supported vanadium catalysts showed remarkable performances for the oxidative coupling (see Table 3). The SiO_2-supported vanadium dimers (self-assembled from the vanadium-monomer precursor) were active and 100% selective for BINOL in both $CHCl_3$ and toluene solutions. The activity in toluene was 1.3 times greater than that in $CHCl_3$. $CHCl_3$ was a better solvent to maximize ee than toluene. However, some vanadyl complexes leached out into the $CHCl_3$ solution after the reaction, whereas no leaching was observed in toluene. Al_2O_3 and TiO_2 were not suitable as supports for the vanadium precursor (see Table 3). On Al_2O_3, the selectivity toward BINOL was only 53% and was not enantioselective (−2%) in $CHCl_3$. The TiO_2-supported vanadium complex did not produce BINOL (0% selectivity). The both supported catalysts produced no BINOL in toluene (not listed).

TABLE 4: Variation of Catalytic Performances and Enantiomeric Excess (ee) of the L-Leucine-Based Vanadium Complexes on SiO_2 in the 2-Naphthol Coupling with Vanadium Loading[a]

vanadium loading (wt %)	time (day)	conversion (%)	selectivity (%)	ee (R) (%)	turnover frequency, TOF (day^{-1})[b]
0.3	5	11	100	32	0.4
0.3[c]	5	10	100	33	
0.8	5	33	100	39	1.2
1.6	5	42	100	48	1.5
3.4	11	93	100	90	1.5
3.4[c]	11	91	100	89	

[a] All the reactions were performed in 5 mL of toluene at 263 K, 100 mg of catalyst were used, and the vanadium dimer/2-naphthol ratio was fixed to $^1/_{36}$. [b] The turnover frequency is a reaction rate defined as the number of BINOL molecules produced per vanadium dimer per day. [c] Reused.

The effect of ligands to enantioselectivity was investigated on the SiO_2-supported vanadium (0.3 wt %) catalysts among six different Schiff-base ligands. TOFs (turnover frequencies), which are defined as the reaction rates of BINOL formation per vanadium dimer, were similar to all the SiO_2-supported vanadium catalysts. A L-valine-based vanadyl complex (5%−14% ee) was less enantioselective, compared to a L-leucine-based complex (32% ee in toluene at 263 K). On the other hand, there is negligible difference between vanadyl complexes prepared from L-isoleucine (51% ee, $CHCl_3$, 263 K), L-leucine (54% ee, $CHCl_3$, 263 K), and L-phenylalanine (56% ee, $CHCl_3$, 263 K). The substitution of salicylaldehyde to hydroxy naphthaldehyde on the L-leucine complex did not lead to an improvement in enantioselectivity (31% ee in toluene at 263 K). The most bulky ligand, L-tert-leucine, reduced the enantioselectivity to 12% ee in toluene at 263 K. The choice of ligands was not a primary factor to determine the enantioselectivity. In toluene without a leaching of vanadyl complexes, the maximum ee was as small as 32% ee for the L-leucine vanadyl complex on SiO_2.

The vanadium loading on SiO_2 including a L-leucine segment was varied over a loading range of 0.3−3.4 wt %, to maximize the enantioselectivity for the coupling reaction (Table 4). No leaching of vanadyl complexes was observed for all the supported catalysts in toluene. With increased vanadium loadings (0.3, 0.8, 1.6, and 3.4 wt %), the enantioselectivity dramatically increased (32%, 39%, 48%, and 90% ee, respectively), as shown in Table 4. The 3.4 wt % vanadium catalyst, which corresponded to full coverage of the vanadyl complex, exhibited 90% ee, which was comparable to the best performance for the coupling of 2-naphthol on a homogeneous catalyst reported thus far. Furthermore, the supported vanadium catalysts can be reused after filtration and exhibited similar catalytic performances, as shown in Table 4.

The reaction rates (TOFs) were proportional to the concentration of 2-naphthol in the concentration range of <0.07 mol/L, as shown in Figure 7, and the TOFs were saturated at the higher concentrations. Thus, the TOFs in Table 4 are dependent on the concentrations of the supported vanadyl complex and the reactant. The catalytic activity per vanadium dimer of the supported vanadyl complexes was independent of the vanadium loading. Because the vanadium loadings of 1.6 and 3.4 wt % correspond to 2-naphthol concentrations of 0.11 and 0.24 mol/L, respectively, the reactions on the catalysts with 1.6 and 3.4 wt % vanadium were conducted in the saturated region (see Figure 7).

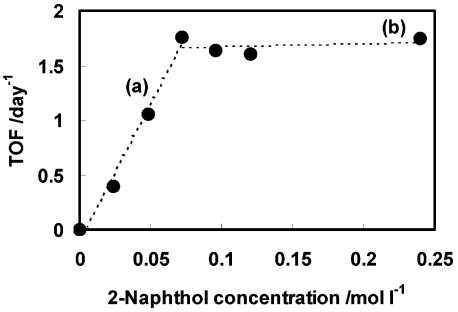

Figure 7. Relationship between the concentration of 2-naphthol and the catalytic activity (turnover frequency, TOF) for the oxidative coupling of 2-naphthol. The catalytic reactions were performed on 100 mg of catalyst with 0.3 wt % vanadium (vanadium dimer content of 3.3×10^{-6} mol) in 5 mL of toluene at 263 K.

TABLE 5: Catalytic Activities of the Supported Vanadium Complex (0.3 wt % Vanadium) for the 2-Naphthol Coupling in the Absence and Presence of O_2[a]

run number	atmosphere[b]	turnover frequency, TOF (day^{-1})
1	O_2	3.6
2	N_2	0.24[c]
3	O_2[d]	3.7

[a] The vanadium dimer/2-naphthol ratio was $^1/_{36}$, the catalyst mass was 100 mg, and the toluene volume was 5 mL. [b] At a pressure of 101.3 kPa. [c] The reaction stopped and no more product was detected for longer reaction. [d] N_2 was evacuated after run 2 and O_2 was admitted to the system.

TABLE 6: Activation Energies, Activation Enthalpies, and Activation Entropies for the Oxidative Coupling of 2-Naphthol on the Supported Vanadium Catalyst (3.4 wt % Vanadium)

solvent	activation energy, E_a (kJ/mol)	activation enthalpy, $\Delta^{\ddagger}H$ (kJ/mol)[a]	activation entropy, $\Delta^{\ddagger}S$ (J K^{-1} mol^{-1})
toluene	47	45	−144
$CHCl_3$	49	47	−140

[a] $\Delta^{\ddagger}H$ was calculated using the following equation: $\Delta^{\ddagger}H = E_a - RT$.

Table 5 shows TOFs on the supported vanadium catalyst in the presence and absence of O_2, and Table 6 shows kinetic parameters such as activation energies, activation enthalpy, and activation entropies for the oxidative coupling of 2-naphthol. The TOF under O_2 was 3.6 day^{-1}. On the other hand, when N_2 was admitted to the same reaction system after evacuation of O_2, the TOF was as slow as 0.24 day^{-1}. The reaction completely stopped and no BINOL was further produced in a prolong reaction. This limited amount of produced BINOL under N_2 may be due to the residual O_2 that remained after the O_2 evacuation. The admission of O_2 to the reaction system recovered the initial catalytic activity to 3.7 day^{-1}. Hence, the presence of O_2 is a prerequisite for the oxidative coupling of 2-naphthol. The activation energies, activation enthalpies, and activation entropies were 47 kJ/mol, 45 kJ/mol, and −144 J K^{-1} mol^{-1}, respectively, in toluene and 49 kJ/mol, 47 kJ/mol, and −140 J K^{-1} mol^{-1}, respectively, in $CHCl_3$. There was no significant solvent effect on these kinetic parameters.

4. Discussion

4.1. Chiral Self-Dimerization of Vanadium Complexes on SiO_2. Assembled structures often provide amazing events in catalysis that are different from those in monomer catalysis, by creating new reaction sites/spaces and controlling dynamic

behavior of metal sites. For examples, rhodium dimeric structures on SiO_2 are crucial to exhibit high catalytic activity for alkene hydrogenation.[34,35] The expanded framework of Ru_6C clusters on MgO is a key issue for H_2/CO reaction to produce oxygen-containing products.[28] Rhodium dimers on SiO_2 that are capable of reversible breaking/regeneration of the Rh−Rh bond are selective for ethene hydroformylation.[29,30] Dimeric cobalt species on Al_2O_3 promote catalytic NO−CO reaction, in contrast to the inactivity of isolated cobalt monomers.[31] Thus, it is ultimately important to explore a new way to design an active assembly of metal complexes on oxide surfaces in a controllable manner.

The vanadium precursors coordinated with Schiff-base ligands are monomeric in alcohol solutions,[67] and two diastereomers exist, because of the two possible directions of V═O, relative to the face of the tridentate ligands. The energy difference between the two diastereomers was calculated to be <1 kJ/mol,[44−46] indicating that the two diastereomers coexist in similar concentrations in solutions. In crystal form, no direct V−V interaction is observed: the shortest interatomic length is 0.6816 nm.[63] There is no attractive force producing a V−V interaction in the structure of the vanadium precursor itself.

The pre-edge position of the V K-edge XANES spectra in Figure 1 and the XPS V 2p binding energies reveal that the vanadium valence in the supported vanadyl complexes remains at 4, which is as same as that of the vanadium precursor. Upon supporting, a V═O bond was preserved, but the symmetry of the vanadyl complexes became distorted, as monitored by the appearance of a d−d transition in the DR−UV/VIS spectra. These behaviors were observed regardless of the amount of vanadium loading. Thus, an increase in vanadium loading on SiO_2 does not cause the distortion of vanadium species. Such distorted structures are typically unstable in solutions and easily decompose during catalytic reactions, although they are catalytically active. The surface, as a large ligand for the metal complexes, not only gives the steric distortion to activate the metal complexes but also prevents such active species from decomposing by immobilizing the metal species.

The EXAFS and FT-IR spectra of the supported vanadyl complexes reveal the a unique surface-attaching reaction that is promoted by surface Si−OH groups. The decrease in the CN of V−O(N) bonds indicates that the vanadium center becomes unsaturated on the surface. The large shift of $\nu_{(Ph-O)}$ and the change in the intensity ratio of $\nu_{(Ph)}$, together with the comparison of FT-IR spectra between Ph−OH and Ph−ONa, demonstrate that the PhO− coordination is dispatched from the vanadium center by the reaction of the vanadium precursor with the Si−OH to form a Ph−OH group, as illustrated in Scheme 1.

The unsaturated vanadium centers were stabilized by the two sets of hydrogen bonding between the two vanadyl complexes, which were the driving force for the self-dimerization of the vanadyl complexes at the surface, as shown by DFT calculations. The ESR spectra for the supported vanadyl complexes in Figure 5 demonstrate the existence of two vanadyl complexes nearby. The vanadium-monomer precursor in solution showed hyperfine signals in ESR spectrum due to V nucleus spin (see Figure 5a), whereas a significant broad signal was observed in addition to the hyperfine signals in Figure 5b. The broad signal indicates that the vanadyl complexes assemble on the surface to cause V−V dipole coupling. The large increase in the intensity of the broad signal and the appearance of a half band by oxygen adsorption (see Figure 5) evidences the dimerization of two vanadium species at a distance of 0.40 ± 0.05 nm. The bond length of O_2 and the average distance of the V−O coordination are 0.111 nm and 0.20−0.21 nm, respectively: therefore, the two V atoms should be located at a distance of >0.40 nm and <0.53 nm. The V−V distance determined by the ESR analysis agrees well with these values. Adsorbed oxygen bridges the two V atoms.

The coupling of two vanadium monomers on a silica cluster was successfully modeled by DFT calculations. Figure 6 visualizes the assembled dimer structure of the L-leucine-based vanadyl complexes, where two monomers are bonded to each other with two sets of hydrogen bonding between the Ph−OH and the carbonyl oxygen of COO. We have examined all possible hydrogen bondings of the Ph−OH with functional groups of the adjacent vanadyl complexes by DFT calculations, for example, Ph-OH···HO−Ph, Ph−OH···O═V, etc. The other combinations for hydrogen bonding did not give reasonable assembled structures. The conformation with two V═O bonds directed toward the outside of these complexes in Figure 6 was the sole model to totally agree with the EXAFS, FT-IR, and ESR data. The electronic delocalization of COO moiety showed a small shift in asymmetric and symmetric COO frequencies (see Table 2). The hydrogen bonding that drives the dimerization relaxes the preservation of free Ph−OH to easily coordinate back to vanadium and maintains the unsaturated structure of the vanadium center to be active for the catalytic coupling reaction. Furthermore, the fixing of the V═O direction by the tridentate ligand in the vanadium dimeric structure causes a fastening chirality on the vanadium center. The isomers cannot be discriminated in solutions. Two chiral isobutyl groups derived from L-leucine overhang outside the assembly, and a chiral reaction space is constructed inside the space that is surrounded by the two vanadyl complexes, as shown in Figure 6.

The behavior of vanadyl complexes on SiO_2 was independent of the vanadium loading, which suggests that the surface vanadyl-complex assembly proceeds even at the low vanadium loading (~0.3 wt %). Surface silanol groups react with the vanadium precursors to form Ph−OH that promotes the dimerization. Note that the chiral self-dimerization of vanadyl complexes coordinated with Schiff bases occurs exclusively on the SiO_2 surface, as promoted by the surface Si−OH. It is a serious problem to create uniform active structures on heterogeneous surfaces for the design of selective heterogeneous catalysts. Particularly, heterogeneous asymmetric catalysis is, to a great extent, damaged by the heterogeneity of surfaces. The catalytic activity of supported catalysts is often derived from the unsaturated property of metal species; however, the removal of ligands to make unsaturated metal centers is fatal to build enantioselectivity, because of a dramatic reduction of the asymmetric field on the metal sites. We have determined that novel chiral self-dimerization of the vanadyl complexes produced the active unsaturated structure with a new chiral conformation on a SiO_2 surface, which occurred on the surface, and provided highly enantioselective active sites for the asymmetric oxidative coupling of 2-naphthol.

4.2. Mechanism for the Oxidative Coupling of 2-Naphthol. The unsaturated vanadium dimer is easily coordinated with 2-naphthol, accompanied with an increase in the CN of V−O (from 3 to 4, as characterized by EXAFS in Table 1). Despite the addition of excess amount of 2-naphthol, a V site accommodates only one 2-naphthol molecule. The coupling reaction for the synthesis of one BINOL molecule requires two 2-naphthol molecules, and the vanadium dimer structure is advantageous to react two 2-naphthol molecules activated on two

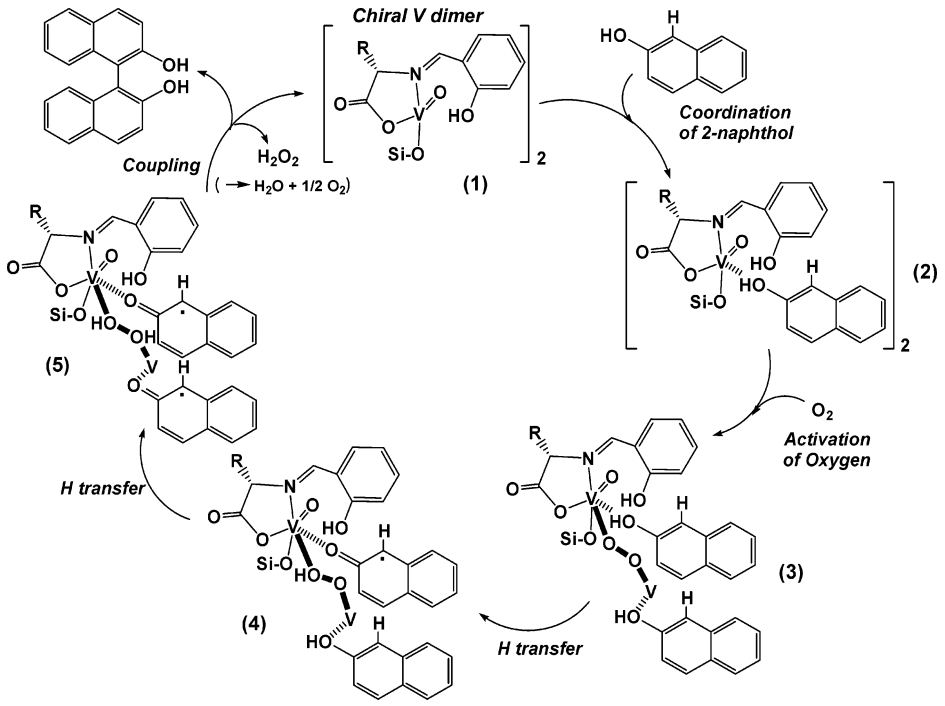

Figure 8. Proposed mechanism for the oxidative coupling of 2-naphthol on the chiral self-dimerized vanadyl complex on SiO_2 under the saturated adsorption of 2-naphthol. A vanadyl complex is simply shown as V in the illustration, to avoid complexity.

adjacent V sites in the vanadium dimer to form BINOL. Monomer structures are entropically disadvantageous for the coupling.

The dimer structure is also efficient to activate oxygen molecules. The dissociation of a strong O═O bond requires extremely unsaturated metal species in low valence states; however, the following reactions often stop, because of too-stable metal−oxygen bonds that are produced after the bond breaking of O═O. Similar amounts of oxygen were adsorbed before and after the coordination of 2-naphthol. Hence, an oxygen molecule weakly adsorbs on the vanadium dimer without losing its reactivity. The catalytic reaction did not proceed in the absence of oxygen. Thus, weakly adsorbed oxygen molecules are suggested to be active species for the hydrogen extraction of 2-naphthol (Figure 8).

A proposed mechanism of the asymmetric oxidative coupling of 2-naphthol is depicted in Figure 8. Initially, 2-naphthol coordinates to an unsaturated V center and then an O_2 molecule adsorbs on the vanadium dimer in a bridging fashion, as indicated from the V−V separation that has been determined by ESR. In the third step, the activated oxygen extracts the H atom of the hydroxyl group of the coordinated 2-naphthol. Finally, two dehydrogenated 2-naphthols couple together to form BINOL in the hollowed slit of the vanadium dimer structure in Figure 6. The 2-naphthol coordination and oxygen adsorption were too fast to monitor the rates; therefore, these two steps are not rate-determining for the coupling reaction. The reaction rate was first-order, in regard to the 2-naphthol concentration, as shown in Figure 7 (region (a)). Hence, it is suggested that the third step, hydrogen transfer from 2-naphthol to the oxygen molecule, is a rate-determining step and the subsequent coupling reaction to form BINOL should be faster. This also implies that the hydrogen abstraction of the second 2-naphthol by the half-hydrogenated oxygen (V−OOH) is much faster than that of the first 2-naphthol in the third step.

4.3. Asymmetric Catalysis of the Chiral Self-Dimerzied Vanadyl Complexes on SiO_2. Enantioselectivity was not modified by the chiral alkyl groups of Schiff-base ligands, as shown in Table 3. We have examined six ligands with different shapes for the vanadium precursors listed in Scheme 1 (also see the Experimental Section). Relatively small L-valine was less enantioselective, and ligands larger than butyl groups were determined to be necessary for the enantioselectivity. However, a sufficient increase in the enantioselectivity was not observed with L-leucine, L-isoleucine, and L-phenylalanine, despite the fact that the size and shape of these amino acids were much different on a size level of methyl and phenyl groups. The most bulky ligand, L-tert-leucine, has a *tert*-butyl group neighboring the V reaction site, but it reduced the enantioselectivity. These two alkyl groups overhung outside the vanadyl complexes illustrated in Figure 6, and they seemingly did not affect the asymmetric coupling of 2-naphthol.

It is worthy to note that the enantioselectivity of the coupling reaction is determined by the chiral conformation on the V center, rather than the chirality of Schiff-base ligands. The chirality of the ligands sterically affects the chiral self-dimerization of vanadyl complexes on the surface, and the chiral ligands themselves do not determine the enantioselectivity for the 2-naphthol coupling. The increase in vanadium loading on SiO_2 achieved the higher regulation of mobility of the assembled vanadium species on the surfaces, resulting in the high enantioselectivity (90% at 93% conversion) on the catalyst with 3.4 wt % vanadium, compared to the case of the catalyst with 0.3 wt % vanadium with the same vanadium structure (see Table 4).

4. Conclusion

The chiral self-dimerization of vanadium-monomer complexes with amino-acid-based Schiff bases was discovered on a SiO_2 surface, which was characterized by ESR, XPS, UV/VIS, FT-IR, XAFS, and DFT. A new chirality was created on the vanadium center by the self-dimerization. The self-assembling was initiated by the reaction of the vanadium monomers with surface Si−OH groups. The hydrogen (proton) of surface silanol was transferred to the Ph−O moiety of the Schiff-base ligand

to form a Ph−OH group, which makes a hydrogen bonding with a carboxyl group of the adjacent vanadium monomer on the surface. The two sets of hydrogen bonding are the origin of the dimerization of two vanadium monomers. ESR spectra in the presence of oxygen demonstrated the assembling of vanadyl complexes at the V−V interatomic distances of $r = 0.40$ ($\pm$ 0.05) nm. The vanadium dimer assembly catalyst exhibited 96% conversion, 100% selectivity to BINOL, and 90% enantioselectivity for the asymmetric oxidative coupling of 2-naphthol, whereas the vanadium precursors themselves were not active for the reaction. The increase in the vanadium loading caused a dramatic increase in the enantioselectivity, up to 90% ee. The supported vanadium catalysts were reusable in toluene. Less acidic and amphoteric oxides, such as Al_2O_3 and TiO_2, were not suitable supports for the vanadium precursors, because they exhibited much lower selectivities (0%−53%) without enantioselectivity (0%). To our knowledge, the vanadium dimer on SiO_2 is the first heterogeneous catalyst for the asymmetric oxidative coupling of 2-naphthol.

Acknowledgment. The XAFS measurements were performed with the approval of the Photon Factory Advisory Committee (PAC) (No. 2004G080). This study was performed with the support of the 21st Century COE Program by the Ministry of Education, Cultures, Sports, Science, and Technology.

References and Notes

(1) (a) Pu, L. *Chem. Rev.* **1998**, *98*, 2405. (b) Chen, Y.; Yekta, S.; Yudin, A. K. *Chem. Rev.* **2003**, *103*, 3155.
(2) (a) Noyori, R. *Asymmetric Catalysis in the Organic Synthesis*; Wiley: New York, 1994. (b) Dalko, P. I.; Moisan, L. *Angew. Chem., Int. Ed.* **2004**, *43*, 5138.
(3) Bao, J.; Wulff, W. D.; Rheingold, A. L. *J. Am. Chem. Soc.* **1993**, *115*, 3814.
(4) Noyori, R.; Takaya, H. *Acc. Chem. Res.* **1990**, *23*, 345.
(5) Blaser, H.-U. *Chem. Rev.* **1992**, *92*, 935.
(6) Kaupp, G. *Angew. Chem., Int. Ed. Engl.* **1994**, *33*, 728.
(7) Pummerer, R.; Rieche, A.; Prell, E. *Chem. Ber.* **1926**, *59*, 2159.
(8) Dewar, M. J. S.; Nakaya, T. *J. Am. Chem. Soc.* **1968**, *90*, 7134.
(9) Feringa, B.; Wynberg, H. *Bioorg. Chem.* **1978**, *7*, 397.
(10) Armengol, E.; Corma, A.; Garcia, H.; Primo, J. *Eur. J. Org. Chem.* **1999**, *64*, 1915.
(11) Kuiling, D.; Yang, W.; Lijun, Z.; Yangjie, W. *Tetrahedron* **1996**, *52*, 1005.
(12) Yamamoto, H.; Fukushima, H.; Okamoto, Y.; Hatada, K.; Nakazaki, M. *J. Chem. Soc. Chem. Commun.* **1984**, 1111.
(13) Nakajima, M.; Miyoshi, I.; Kanayama, K.; Hashimoto, S.-I. *J. Org. Chem.* **1999**, *64*, 2264.
(14) Lin, X.; Yang, J.; Kozlowski, M. C. *Org. Lett.* **2001**, *3*, 1137.
(15) Irie, R.; Matsutani, K.; Katsuki, T. *Synlett* **2000**, 1433.
(16) Chu, C. Y.; Hwang, D. R.; Wang, S. K.; Uang, B. J. *Chem. Commun.* **2001**, 980.
(17) Hon, S. W.; Li, C. H.; Kuo, J. H.; Barhate, N. B.; Liu, Y. H.; Wang, Y.; Chen, C. T. *Org. Lett.* **2001**, *3*, 869.
(18) Luo, Z.; Liu, Q.; Gong, L.; Cui, X.; Mi, A.; Jiang, Y. *Chem. Commun.* **2002**, 914.
(19) Luo, Z.; Liu, Q.; Gong, L.; Cui, X.; Mi, A.; Jiang, Y. *Angew. Chem., Int. Ed.* **2002**, *41*, 4532.
(20) Somei, H.; Asano, Y.; Yoshida, T.; Takizawa, S.; Yamataka, H.; Sasaki, H. *Tetrahedron Lett.* **2004**, *45*, 1841.
(21) Iwasawa, Y. *Adv. Catal.* **1987**, *35*, 187.
(22) Iwasawa, Y. *Acc. Chem. Res.* **1997**, *30*, 103.
(23) Iwasawa, Y. *Stud. Surf. Sci. Catal.* **1996**, *101*, 21.
(24) Iwasawa, Y. *Tailored Metal Catalysts*; Reidel: Dordrecht, The Netherlands, 1986.
(25) Tada, M.; Iwasawa, Y. *J. Mol. Catal. A: Chem.* **2003**, *199*, 115.
(26) Tada, M.; Iwasawa, Y. *J. Mol. Catal. A: Chem.* **2003**, *204−205*, 27.
(27) Suzuki, A.; Tada, M.; Sasaki, T.; Shido, T.; Iwasawa, Y. *J. Mol. Catal. A: Chem.* **2002**, *182−183*, 415.
(28) Izumi, Y.; Chihara, H.; Yamazaki, H.; Iwasawa, Y. *J. Phys. Chem.* **1994**, *98*, 594.
(29) Asakura, K.; Bando, K. K.; Iwasawa, Y.; Arakawa, H.; Isobe, K. *J. Am. Chem. Soc.* **1990**, *112*, 9096.
(30) Bando, K. K.; Asakura, K.; Arakawa, H.; Isobe, K.; Iwasawa, Y. *J. Phys. Chem.* **1996**, *100*, 13636.
(31) Shido, T.; Yamaguchi, A.; Asakura, K.; Iwasawa, Y. *J. Mol. Catal. A: Chem.* **2000**, *163*, 67.
(32) Asakura, K.; Noguchi, Y.; Iwasawa, Y. *J. Phys. Chem. B* **1999**, *103*, 1051.
(33) Tada, M.; Sasaki, T.; Iwasawa, Y. *Phys. Chem. Chem. Phys.* **2002**, *4*, 4561.
(34) Tada, M.; Sasaki, T.; Shido, T.; Iwasawa, Y. *Phys. Chem. Chem. Phys.* **2002**, *4*, 5899.
(35) Tada, M.; Sasaki, T.; Iwasawa, Y. *J. Catal.* **2002**, *211*, 496.
(36) Tada, M.; Sasaki, T.; Iwasawa, Y. *J. Phys. Chem. B* **2004**, *108*, 2918.
(37) Tada, M.; Shimamoto, M.; Sasaki, T.; Iwasawa, Y. *Chem. Commun.* **2004**, 2562.
(38) Vilter, H. *Phytochemistry* **1984**, *23*, 1387.
(39) Arber, J. M.; de Boer, E.; Garner, C. D.; Hansnain, S. S.; Wever, R. *Biochemistry* **1989**, *28*, 7968.
(40) Robson, R. L.; Eady, R. R.; Richardson, T. H.; Miller, R. W.; Hawkins, M.; Postgate, J. R. *Nature* **1986**, *322*, 388.
(41) George, G. N.; Coyle, C. L.; Hales, B. J.; Cramer, S. P. *J. Am. Chem. Soc.* **1988**, *110*, 4057.
(42) Hales, B. J.; True, A. E.; Hoffman, B. M. *J. Am. Chem. Soc.* **1989**, *111*, 8519.
(43) Tada, M.; Taniike, T.; Kantam, L. M.; Iwasawa, Y. *Chem. Commun.* **2004**, 2542.
(44) Cundari, T. R.; Sisterhen, L. L.; Stylianopoulos, C. L. *Inorg. Chem.* **1997**, *36*, 4029.
(45) Cundari, T. R.; Saunders: L.; Stylianopoulos, C. L. *J. Phys. Chem. A* **1998**, *102*, 997.
(46) Pessoa, J. C.; Calhorda, M. J.; Cavaco, I.; Correia, I.; Duarte, M. T.; Felix, V.; Henriques, R. T.; Piedade, M. F. M.; Tomaz, I. *J. Chem. Soc., Dalton Trans.* **2002**, 4407.
(47) Theriot, L. J.; Carlisle, G. O.; Hu, H. J. *J. Inorg. Nucl. Chem.* **1969**, *31*, 2841.
(48) Eaton, S. S.; More, K. M.; Sawant, B. M.; Eaton, G. R. *J. Am. Chem. Soc.* **1983**, *105*, 6560.
(49) Velayutham, M.; Varghese, B.; Subramanian, S. *Inorg. Chem.* **1998**, *37*, 1336.
(50) Forrest, J. G.; Prout, C. K. *J. Chem. Soc. Sect. A* **1967**, 1312.
(51) Tapscott, R. E.; Belford, R. L. *Inorg. Chem.* **1967**, *6*, 735.
(52) Wong, J.; Lytle, F. W.; Messemer, R. P.; Maylotte, D. H. *Phys. Rev. B* **1984**, *30*, 5596.
(53) Stern, E. A.; Newville, M.; Ravel, B.; Yacoby, Y.; Haskel, D. *Phys. B (Amsterdam, Neth.)* **1995**, *208−209*, 117.
(54) Ankudinov, A. L.; Ravel, B.; Rehr, J.; Conradson, S. D. *Phys. Rev. B* **1998**, *58*, 7565.
(55) Delley, B. *J. Chem. Phys.* **1990**, *92*, 508.
(56) Perdew, J. P.; Wang, Y. *Phys. Rev. B* **1992**, *45*, 13244.
(57) Stizza, S.; Mancini, G.; Benfatto, M.; Natoli, C. R.; Garcia, J.; Bianconi, A. *Phys. Rev. B* **1989**, *40*, 12229.
(58) Horvath, B.; Strutz, J.; Geyer-Lippmann, J.; Horvath, E. G. *Z. Anorg. Allg. Chem.* **1981**, *483*, 181.
(59) Sawatzky, G. A.; Post, D. *Phys. Rev. B* **1979**, *20*, 1546.
(60) Larsson, R.; Folkesson, B.; Schoen, G. *Chem. Scr.* **1973**, *3*, 88.
(61) Casella, L.; Gullotti, M. *J. Am. Chem. Soc.* **1981**, *103*, 6338.
(62) Pessoa, J. C.; Cavaco, I.; Correia, I.; Duarte, M. T.; Gillard, R. D.; Henriques, R. T.; Higes, F. J.; Madeira, C.; Tomaz, I. *Inorg. Chem. Acta* **1999**, *293*, 1.
(63) Rehder, D.; Schulzke, C.; Dan, H.; Meinke, C.; Hanss, J.; Epple, M. *J. Inorg. Biochem.* **2000**, *80*, 115.
(64) Basu, P.; Pal, S.; Chakravorty, A. *J. Chem. Soc., Dalton Trans.* **1991**, 3217.
(65) Cornman, C. R.; Kampf, J.; Lah, M. S.; Pecoraro, V. L. *Inorg. Chem.* **1992**, *31*, 2035.
(66) Hausan, G. R.; Kabanos, T. A.; Kevamidas, A. D.; Mentzafos, D.; Terzis, A. *Inorg. Chem.* **1992**, *31*, 2857.
(67) Cavaco, I.; Pessoa, J. C.; Duarte, M. T.; Henriques, R. T.; Matias, P. M.; Gillard, R. D. *J. Chem. Soc., Dalton Trans.* **1996**, 1989.